IET Nanobiotechnology

Research Article

IET Journals
The Institution of Engineering and Technology

Biosynthesis of eco-friendly and recyclable Pd/LDHs catalyst using the withered leaves extract for Suzuki coupling reaction

ISSN 1751-8741
Received on 31st May 2019
Revised 25th August 2019
Accepted on 26th September 2019
E-First on 3rd January 2020
doi: 10.1049/iet-nbt.2019.0188
www.ietdl.org

Xizheng Fan[1] ✉, *Yanyan Zheng*[1]

[1]*Shandong Chambroad Petrochemicals Co. Ltd, Binzhou 256600, Shandong Province, People's Republic of China*

✉ *E-mail: fxzfxzfglfgl@126.com*

Abstract: The hydrotalcite-supported palladium (Pd) catalyst is prepared with a green and environmentally friendly route, introducing the extract of withered leaves as a dispersant and reducing agent (Pd/LDHs-B). Compared with the as-prepared catalyst (Pd/LDHs-P with the average diameter of 4.3 nm) using a chemical synthesis method with polyvinylpyrrolidone as a dispersant and ascorbic acid (Vc) as a reductant, the results indicate that the size of Pd nanoparticles in Pd/LDHs-B is smaller (ca. 3.6 nm). The Pd-LHDs-B (0.5 mmol‰) exhibits higher activity (98.66%) than Pd/LDHs-P (98.19%) in the Suzuki reaction of 4-bromotoluene and phenylboronic acid at 60°C for 30 min. Also, the reusability of Pd/LDHs-B is confirmed by recycling tests without a significant decrease in activity.

1 Introduction

Palladium (Pd) catalyst has been intensively studied as the highly efficient catalyst in the region of organic synthesis for Suzuki coupling reaction [1–4], with high-power for the construction of C–C bonds to synthesise biaryl unit, which is applied to the fields of natural products [5], pharmaceutical intermediates [6, 7] and advanced functional materials [8, 9].

Heterogeneous Pd nano-catalysts [10, 11] with easy reclamation have drawn more attention than homogeneous catalysts. In order to increase the efficiency of the catalysts, the chemical reagents are frequently used to disperse and reduce Pd ions in the procedure of traditional Pd catalysts, which have the toxicity and cause the pollution to the environment easily. In addition, physical preparation methods including ultrasound and plasma [12, 13] have been developing which require more expensive instruments and more energy. In contrast, with the promotion of environmental protection and green chemistry concept, pathfinders are exploring reliable, eco-friendly and promising processes for the synthesis of metal catalysts. Therefore, the widespread existing plants as a source of promising biomass have aroused great interest in the preparation of advanced catalytic materials [14–17]. The biosynthetic method has been characterised by simple production, waste utilisation, no chemical pollutants, and low cost. In 2014, Lu *et al.* [18] adopted a plant-mediated synthetic method to prepare Ag–Pd alloy nano-catalyst by the extract of *Platycladus* leaves, which provides high activity in the hydrogenation reaction of 1,3-butadiene. Now nano-metal catalysts containing Pt, Ni, Au, Ag etc. [19–22] have been prepared with the safe and pollution-free protocol using the biomass of poplar, sea-buckthorn, pine and so on.

As we all know, the readily visible leaves of broadleaf trees will recyclically fall in autumn, which have little application and even are burnt as waste. However, the biological components of the fallen leaves still contain some sugars, phenols and amino acids (AA), which can offer the complexation and antioxidant capacity with Pd metal. Meanwhile, the magnesia–alumina hydrotalcite [23, 24] only prepared by the inorganic salts is a non-toxic and harmless material, which can serve as the environment-friendly supporter for the green synthesis of nano-catalysts.

In this work, the Pd/LDHs-B catalyst using hydrotalcite with a double-layer structure as the supporter is synthesised with the water-soluble extract of the just-fallen *willow* leaves as the dispersing and reducing reagents to replace the complex organic chemical agents (Fig. 1). It is exhilarated that the Pd/LDHs-B in the Suzuki coupling reaction has exhibited superior activity. For comparison, the Pd/LDHs-P is also prepared by a traditional chemical method.

2 Experimental

2.1 Materials and reagents

Pd chloride was used as the Pd source. All the reagents were pure reagents and purchased from Sinopharm Chemical Reagent Co., Ltd. The withered leaves are very common and easy to obtain, which are mainly from broad-leaved trees such as willows, poplars, birches, eucalyptus etc. The withered willow leaves (WWL) were used in this study.

2.2 Extract of the withered leaves

The withered leaves collected under the tree was washed three times with the deionised water and dried in a dark and cool place. Then the dried leaves were pulverised and soaked in the water at 60°C for 1 h and filtered to obtain leachate (the ratio of leaf to water is 5 g:100 g) which was reserved in a brown bottle at 4°C for the preparation of the catalyst.

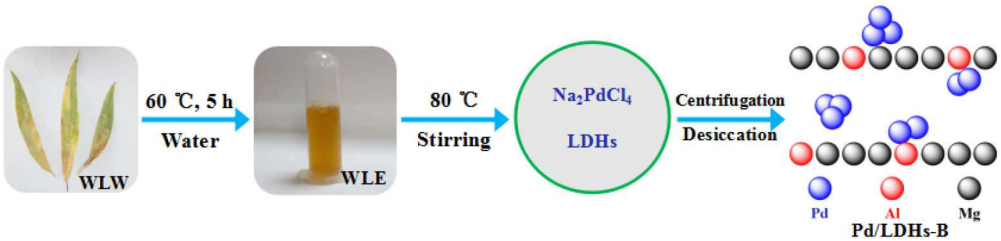

Fig. 1 *Prepared route of Pd/LDHs-B catalyst by the withered leaves extract*

© The Institution of Engineering and Technology 2019

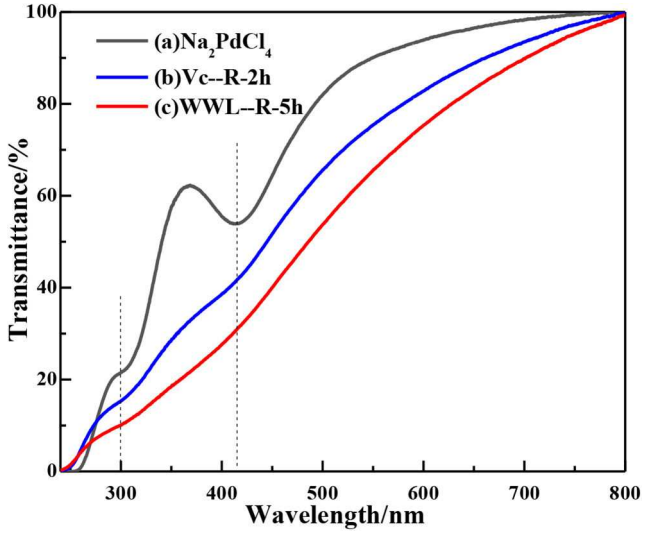

Fig. 2 *UV–Vis spectroscopic images of*
(a) Na_2PdCl_4; nano-Pd reduced by *(b)* Vc, *(c)* WWL

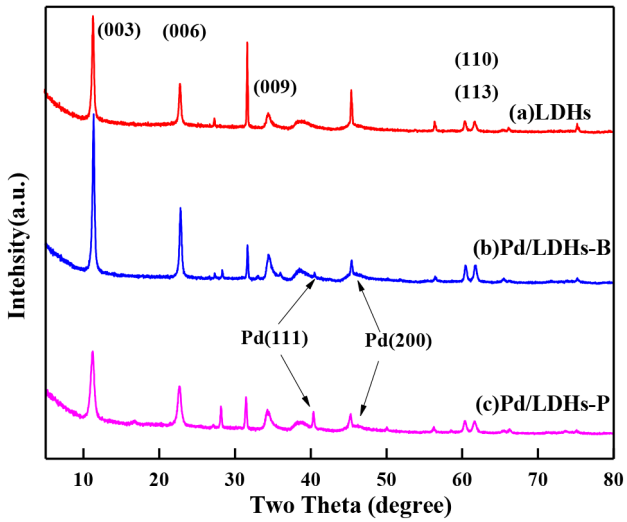

Fig. 3 *XRD patterns of*
(a) LDHs, *(b)* Pd/LDHs-B, *(c)* Pd/LDHs-P

2.3 Preparation of Pd/LDHs catalyst

According to the co-precipitation method [25], the Mg/Al hydrotalcite was prepared as a carrier. The catalyst was prepared in the following steps: first, an aqueous solution of Na_2PdCl_4 at a concentration of 0.02 mol/l was used as a precursor, and the as-prepared hydrotalcite (1.0 g) was weighed into the Na_2PdCl_4 (9.4 ml) solution, according to a certain mass ratio of Pd and hydrotalcite carrier, and impregnated for 6 h in a normal temperature aqueous phase. Second, the 10 ml extract was added drop wise and stirred for another 4 h. Immediately, the temperature was risen to 80°C by the boiling water bath heating method and stirred for reduction. After 5 h, the mixture was filtered and washed thrice by deionised water and dried at 60°C to obtain the supported nano-Pd catalyst (the amount of Pd was 2.0 wt.%), which was named as the Pd/LDHs-B.

In order to verify the activity of catalyst, using polyvinylpyrrolidone (PVP) and vitamin C as the dispersants and the reducing agents, the Pd catalyst was prepared with the same procedure mentioned above under a molar radio of Pd:PVP:AA was 1:12:1.2 at 60°C for 2 h, which was signed as the Pd/LDHs-P with the same Pd amount.

2.4 Catalyst characterisation

The infrared spectroscopy was obtained by the Nicolet 6700 of Fourier transform infrared spectrometer, Nicolet, USA. X-ray diffraction (XRD) patterns of the catalysts were characterised by a Japanese D/max-IIIB X-ray powder diffractometer, with a Cu target (Kα), scanning range 5–80°, and 40 kV voltage and 40 mA current. The photographs of transmission electron micrograph (TEM) were from the German FEI company Tecnai G2 S-TWIN, which had the 200 kV acceleration voltage. The microstructural diagrams of catalysts were characterised by an American Conta Autosorb-iQ physical adsorption instrument test, degassing treatment conditions: 300°C, 180 min, heating rate: 10°C/min. The analytical results of X-ray photoelectron spectroscopy (XPS) were obtained from a Kratos AXIS ULTRA DLD spectrometer with the monochromatic Al Kα (1486.6 eV) radiation. A UV-2450 UV-visible spectrophotometer with a wavelength of 240–800 nm at a resolution of 0.5 nm told us that the bivalent Pd was reduced zero-valent Pd completely or not.

2.5 Catalyst performance test

The performance of the catalyst was verified by the yield of the target product in the Suzuki coupling reaction. The specific steps were as follows: Aryl halide (5.0 mmol), EtOH (25 ml), K_2CO_3 (10 mmol) and H_2O (25 ml) were successively added into a glass tube with a stopper and mixed equably by the magnetic stirring at room temperature. When the temperature rose to 60°C, the Pd/LDHs catalyst (0.5 mmol‰) and phenylboronic acid (7.5 mmol) were added into the mixture. At last, after 30 min, the products were obtained by extracting with ethyl acetate. The evaluation yield was confirmed by high performance liquid chromatography.

2.6 Catalyst recycle

Catalyst reusability was evaluated by multiple reactions, which were based on phenylboronic acid and 4-bromotoluene as the substrates. The catalyst was recovered by filtration and washing twice with ethanol and deionised water and reused for the next reaction.

3 Results and discussion

3.1 Ultraviolet–visible (UV–Vis)

In order to determine the content of the active ingredient in the biomass extract for reduction, we use the gallic acid to determine the amounts of phenolic content in the WWL with the Graham method [26, 27] by ultraviolet–visible (UV–Vis) spectroscopy. A standard curve is established, which is shown in the Appendix. This method helps us to calculate the phenol content of the extract in the Appendix under different conditions.

The UV–Vis spectrophotometer is also used to acquire the process of bio-reduction reaction (Fig. 2) by lots of experiments to determine the effects of temperature and time. The reaction conditions of Pd(II) with two substances (Vc and WWL) have been obviously recorded: the colours of the solutions gradually turn from brownish into dark; the absorption bands of Pd^{2+} at 300 and 420 nm [28], and the light transmittance of liquid fade away, which reveals the Pd(II) ions are reduced to Pd(0). Therefore, we get a suitable condition, which shows that the optimal time and temperature of Vc and WWL for preparing Pd-nanoparticles (NPs), respectively, need 2 h at 60°C and 5 h at 80°C.

3.2 XRD analysis

The wide-angle XRD patterns of LDHs, Pd/LDHs-B, Pd/LDHs-P are shown in Fig. 3. The diffraction peaks at 11.40° (003), 22.78° (006), 34.66° (009), especially the double peaks (60.60° (110) and 62.04° (113)), display that the typical structure of hydrotalcite is subsistent in all samples. The diffraction peaks of Pd at 40.1° and 46.6° found in all of Pd/LDHs-B and Pd/LDHs-P except LDHs describe that the catalysts have mainly (111) lattice plane and a little amount of (200) lattice plane. Comparatively, the diffraction peaks of Pd/LDHs-B have a weaker intensity than Pd/LDHs-P, which testifies that the size of the NPs may be smaller in Pd/LDHs-B prepared by the extractive.

© The Institution of Engineering and Technology 2019

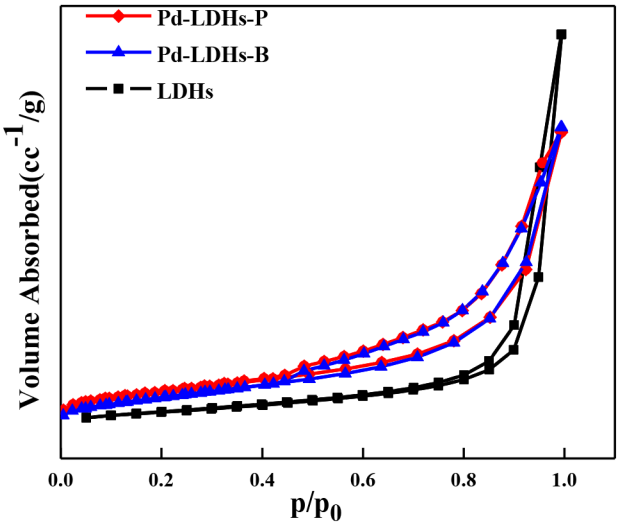

Fig. 4 *N_2 adsorption–desorption isotherms of LDHs; Pd/LDHs-B and Pd/LDHs-P*

Table 1 Pore structure parameters of LDHs, Pd/LDHs-B, and Pd/LDHs-P

Sample	SSA[a], m^2/g	Pore, cm^3/g	Pore diameter, nm
LDHs	148	0.480	15.05
Pd/LDHs-B	114	0.346	9.15
Pd/LDHs-P	122	0.363	9.74

[a]Specific surface area calculated by the Brunauer–Emmett–Teller (BET) method.

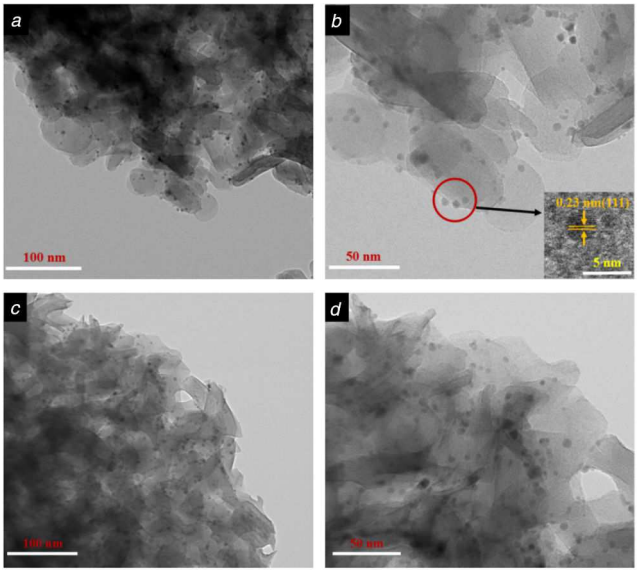

Fig. 5 *TEM images of*
(a), (b) Pd/LDHs-B, ***(c), (d)*** Pd/LDHs-P

3.3 N_2 adsorption–desorption

The pore structures of LDHs, Pd/LDHs-B, Pd/LDHs-P analysed by N_2 adsorption–desorption isotherms are shown in Fig. 4 and Table 1, which illustrate the hydrotalcite is a typical mesoporous material. The characteristic isotherm of the supported hydrotalcite is corresponding to a type IV isotherm with a type H3 hysteresis loop according to the IUPAC classification. The parameters of Pd/LDHs-B, Pd/LDHs-P in Table 1, manifest the decline tendency compared with LDHs (the specific surface area from 148 to 114 and 122 m^2/g; and the pore size from 0.48 to 0.346 cm^3/g, 0.363 cm^3/g). This exhibits that Pd/LDHs-B has a little more marked reduction. Simultaneously, the pore diameter of catalysts containing the Pd decrease, respectively, from 15.05 to 9.15 and 9.74 nm. All these indicate that the structure of the two catalysts is similar. In brief, it suggests that the Pd NPs of Pd/LDHs-B, Pd/LDHs-P are successfully loaded into the carrier and do not destroy the overall structure of the hydrotalcite.

3.4 TEM analysis

The TEM images of Pd/LDHs-B (Figs. 5*a* and *b*) and Pd/LDHs-P (Figs. 5*c* and *d*) exhibit the structure of hydrotalcite and the morphology of Pd NPs in the catalyst. The sheet structure of hydrotalcite is clearly shown in the figures, which is identical to the literature reported by the authors. Meanwhile, near spherical NPs can be found on the hydrotalcite carriers, which is in accordance with the conclusion of the above XRD analysis by measuring the lattice size of NPs (2.3 Å). According to the particle size distribution, the average particle size of Pd/LDHs-B is determined to be 3.6 nm, with the narrow distribution range from 1.2 to 5.3 nm (Fig. 12*a* in the Appendix), which is far less than the pore of LDHs determined by the characterisation of N_2 adsorption–desorption. Similarly, the NPs of Pd/LDHs-P are clearly visible and dispersed evenly with the size range of 1.5–6.6 nm (the average diameter is 4.3 nm shown in Fig. 12*b* in the Appendix). The reason for the Pd/LDHs-P having slightly larger NPs than Pd/LDHs-B is that Vc has a stronger reducing ability, which has been confirmed in the UV. Both catalysts are much smaller than the particle size of the Pd/LDHs catalysts prepared in the liquid phase system without the surfactants that were reported in the literature [25, 29]. These phenomena reveal that the biomass extract not only plays a reducing role but also has a certain dispersion protection effect as the dispersing agent, which can effectively prevent the agglomeration of the nano-Pd particles. Consequently, We obtain a Pd catalyst with smaller particle sizes in an eco-friendly and inexpensive way.

3.5 XPS analysis

The binding energy values shown in Fig. 6 are 335.8 eV for Pd^0 (3d 5/2) and 341.3 eV for Pd^0 (3d 3/2), while the 337.8 eV (3d 5/2) and 342.9 eV (3d 3/2) are assigned to Pd^{2+} in the Pd/LDHs-B. By the integration method to calculate the area of the peak, the ratio of Pd^0 is 71.08%. On the one hand, the reason for the presence of Pd^{2+} is an incomplete reduction of Pd^{2+} ions under the reaction conditions. On the other hand, hydrotalcite contains a large number

© The Institution of Engineering and Technology 2019

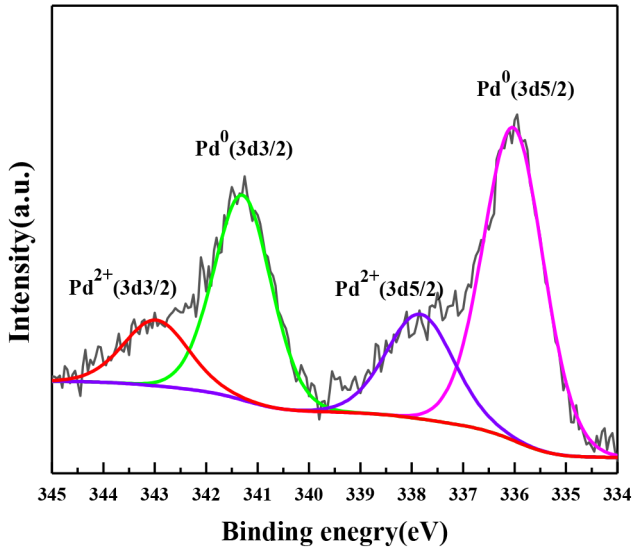

Fig. 6 *XPS spectrum of Pd in Pd/LDHs-B*

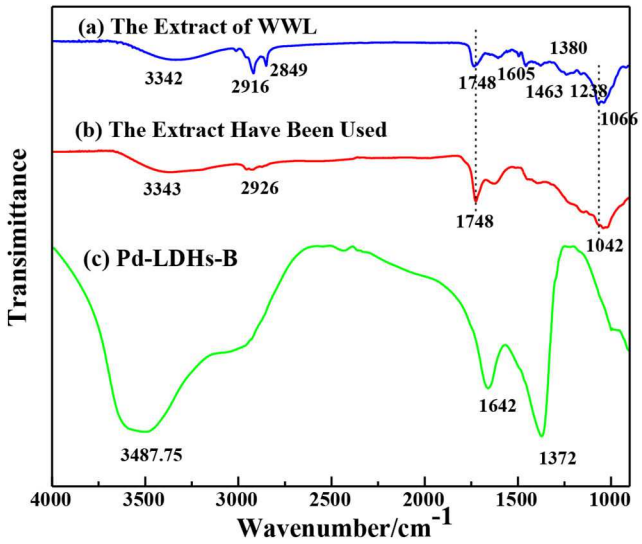

Fig. 7 *FTIR spectra of*
(a) Extract of WWL, ***(b)*** Extract after being used, ***(c)*** Pd/LDHs-B

of oxygen atoms that can interact with Pd and prevent the peripheral Pd atoms from being reduced to Pd^0, which is manifested as some articles reported the catalysts of Pd/LDHs [30, 31]. Effectively, these results demonstrate that most of the Pd^{2+} were reduced into the metallic simple substance by the method of Section 2.3 with the withered leaves extract.

3.6 Fourier transform infrared (FTIR) analysis

Fig. 7 shows the FTIR measurement of the samples used to analyse possible functional groups responsible for each substance, which can identify the impacts of the bio-extract and PVP for the atoms and NPs of Pd. It can be found that the infrared absorption peaks of the extract are observed at 3342, 2916, 2849, 1748, 1605, 1463, 1380, 1238, and 1066 cm^{-1}, corresponding to the various functional groups, respectively. Commonly, the wide peak at 3342 cm^{-1} is assigned to the O–H stretching vibration existing in the saccharide, alcohol and phenolic compounds of broad-leaved plants. The sharp peaks at 2916 and 2849 cm^{-1} are C–H stretching vibration. The peak at 1605 cm^{-1} is identified as the benzene ring in the aromatic compound. The presence of the $–CH_2$ and $–CH_3$ bonds in the extract is determined by the presence of two bending vibration peaks at 1463 and 1380 cm^{-1}. In the end, the –C–O bond is signed by 1238 and 1066 cm^{-1} vibration peak and –C=O is proven by 1748 cm^{-1}, which are identified that the extract contains the alcohol, phenolic, ketone, and aldehyde. Comparing with PVP, the extract also containing C, O, N elements [32, 33], has the same scattered effect that can prevent the Pd agglomeration. Also, the –O–H of saccharide, alcohol, phenolic, e.g. can reduce Pd^{2+} to Pd^0 such as the impact of ascorbic acid, which can be proved by comparing the change of peak at 1066 and 1748 cm^{-1} (the intensity of peaks decrease and increase, respectively) after the biosynthetic reaction in Figs. 7*a* and *b*. This indicates that a part of hydroxyl groups are converted to carbonyl groups after completing the reaction. Finally, the biomass can be wiped off by deionised water, accompanied by the disappearance of several peaks (shown in Fig. 7*c*).

According to the above characterisation results, and combined with the existing literature reports [27, 34], we speculate the mechanism of action of the biomass and Pd as follows in Fig. 8.

3.7 Catalytic evaluation

In order to test the activity of the present catalysts in the Suzuki coupling reaction and explore the optimal reaction conditions, we select 4-bromotoluene and phenylboronic acid as substrates for the probe reaction. The results are summarised in Table 2. The entries of 1–4 suggest that the strong alkali can give the high yield of biphenyl substitution with a yield of over 97%, and the NaOAc, $NH_3{\cdot}H_2O$, and Et_3N (Table 2, entries 5–7) cannot provide sufficient strength of bases in Suzuki coupling reaction depending

© The Institution of Engineering and Technology 2019

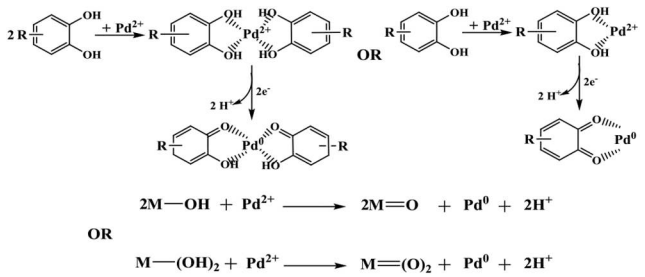

Fig. 8 *Mechanism of the green synthesis for PdNRs*

Table 2 Effect of base and solvents in the Suzuki coupling reaction

Entry	Base	Solvents*	Yield[a], %	Yield[b], %
1	NaOH	CH_3CH_2OH	97.36	97.20
2	KOH	CH_3CH_2OH	98.01	96.79
3	K_2CO_3	CH_3CH_2OH	98.66	98.19
4	$K_3PO_4{\cdot}3H_2O$	CH_3CH_2OH	98.69	97.25
5	NaOAc	CH_3CH_2OH	87.25	86.26
6	$NH_3{\cdot}H_2O$	CH_3CH_2OH	36.26	22.64
7	Et_3N	CH_3CH_2OH	62.64	87.65
8	K_2CO_3	CH_3OH	98.73	98.00
9	K_2CO_3	THF	42.92	24.94
10	K_2CO_3	DMF	33.06	24.43
11	K_2CO_3	DMAc	29.47	32.69
12	K_2CO_3	Toluene	20.81	12.23

Reaction conditions: 4-bromotoluene (5.0 mmol), phenylboronic acid (7.5 mmol), Pd NPs (0.5 mmol ‰), base (10.0 mmol), solvent/H_2O (25 ml/25 ml) at 60°C for 30 min.

[a]Pd-LDHs-B.

[b]Pd-LDHs-P.

*The different organic reagents added in the mixture containing 1:1 volume ratio of H_2O and organic reagents are only listed.

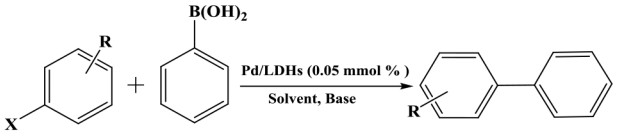

Fig. 9 *Suzuki coupling reactions of aromatic halogenates and phenylboronic acid*

on the mechanism of Suzuki reaction [35, 36]. The results of Pd/LDHs-B and Pd/LDHs-P show that safe and cheap K_2CO_3 gives the best yield. In the same way, we got the best solvent is EtOH/H_2O (non-poisonous and inexpensive as well as K_2CO_3) by comparing it with CH_3OH, tetrahydrofuran (THF), dimethylformamide (DMF), DMAc, and toluene (Table 2, entries 8–12).

Also, we explore the best time, temperature, and Pd dosage for the reaction, which are 30 min, 60°C, and the lowest catalyst dosage of 0.5 mmol‰. These show that as-prepared Pd/LDHs-B and Pd/LDHs-P are all the efficient catalysts with little different yield. It also has a certain increasing yield for different substrates including o-, p-, and m-bromided and p-chlorinated aromatics (shown in Fig. 9 and Table 3) in the Suzuki coupling reaction.

3.8 Catalyst repeatability

The reusability is an important criterion of the catalyst, which can greatly reduce the costs for industrial applications. It is tested by the Suzuki coupling reaction of 4-bromotoluene and phenylboronic acid as the substrates. Since the structures are similar, consistent with the results of XRD, TEM, and N_2-adsorption–desorption, the Pd/LDHs-B and Pd/LDHs-P exhibit similar catalytic activities in Fig. 10. The yield of biphenyl is significantly higher than 92% over four cycles, and the obvious loss in the fifth run is observed to be 88.5%. This is attributed to the loss of some bivalent Pd and a bit aggregation of the particles to become larger. However, after six recycles, the activity still remains at 84%, due to the smaller particle size and the layered structure of hydrotalcite fixed Pd.

4 Conclusions

To summarise, the efficient and recyclable Pd/LDHs-B catalyst is successfully prepared by an eco-friendly and inexpensive method using the extract of withered leaves. It has been demonstrated that the biomass can afford a dual role of dispersion and reduction as PVP and ascorbic acid for Pd ions by analytical tools of XRD, FTIR, and TEM. So the Pd/LDHs-B containing the smaller Pd NPs (mean size of 3.6 nm), exhibits excellent catalytic activity in Suzuki coupling reaction and also can be repeated six times without obvious activity loss attributing to good stability. Importantly, this provides a ‘green chemistry’ method which is a new application of withered leaves in the synthesis of repeatable metal catalysts.

© The Institution of Engineering and Technology 2019

Table 3 Catalysing the Suzuki reactions of different substrate

Entry	R	X	Time, h	*T*, °C	Yield[a], %	Yield[b], %
1	H	Br	0.5	60	96.49	96.91
2	4-NO_2	Br	0.5	60	98.78	97.81
3	4-$COCH_3$	Br	0.5	60	99.04	98.85
4	4-CN	Br	0.5	60	91.19	90.83
5	4-CHO	Br	0.5	60	94.27	92.70
6	4-OCH_3	Br	0.5	60	97.87	92.07
7	4-CH_3	Br	0.5	60	98.66	98.19
8	2-CH_3	Br	0.5	60	66.32	64.30
9	2-OCH_3	Br	0.5	60	75.41	76.72
10	3-NO_2	Br	0.5	60	95.30	90.03
11	4-H	Cl	12	60	39.22	32.57
12	4-NO_2	Cl	12	60	51.23	49.89
13	4-$COCH_3$	Cl	12	60	44.18	43.43

Reaction conditions: aromatic halogenates (5.0 mmol), phenylboronic acid (7.5 mmol), Pd-LDHs (0.5 mmol‰), K_2CO_3 (10.0 mmol), EtOH/H_2O (25 ml/25 ml) at 60°C for 30 min.

[a]Pd-LDHs-B.

[b]Pd-LDHs-P.

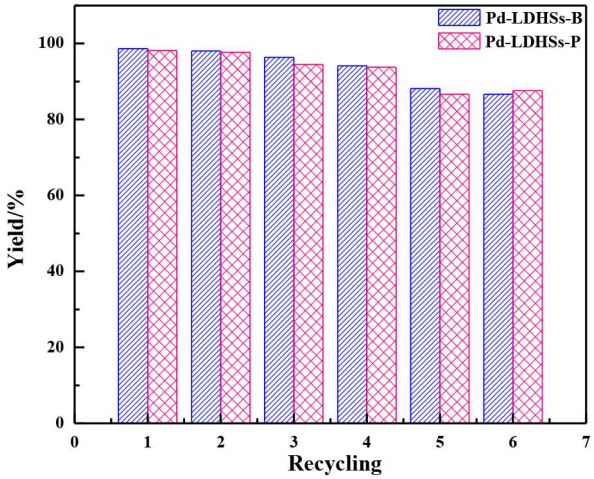

Fig. 10 *Recycling of Pd/LDHs-B and Pd/LDHs-P for the Suzuki coupling reaction*

5 References

[1] Wang, J., Bai, J., Liang, H., *et al.*: 'Photothermal catalytic effect of Pd–TiO_2/CNFs composite catalyst in Suzuki coupling reaction', *Colloids Surf. A*, 2019, **572**, pp. 283–289

[2] Hojat, V., Ahmad, N., Nasim, A., *et al.*: 'Suzuki–Miyaura reaction by heterogeneously supported Pd nanoparticles on thio-modified multi walled carbon nanotubes as efficient nanocatalyst', *Polyhedron*, 2019, **162**, pp. 240–244

[3] Panahi, L., Reza Naimi-Jamal, M., Mokhtari, J.: 'Ultrasound-assisted Suzuki–Miyaura reaction catalyzed by Pd@Cu_2(NH_2–BDC)$_2$(DABCO)', *J. Organomet. Chem.*, 2018, **868**, pp. 36–46

[4] Sun, C., Sun, K., Tang, S.: 'Extended Stöber method to synthesize core–shell magnetic composite catalyst Fe_3O_4@C–Pd for Suzuki coupling reactions', *Mater. Chem. Phys.*, 2018, **207**, pp. 181–185

[5] Kum, D.Y., Nazari, M., McPhail, K.L., *et al.*: 'Two-step total synthesis of an anti-MRSA and myosin-inhibiting marine natural product pentabromopseudilin via Suzuki–Miyaura coupling of a MIDA boronate ester', *Tetrahedron Lett.*, 2017, **58**, pp. 3374–3376

[6] Xie, L., Cui, J., Qian, X., *et al.*: '5-Non-amino aromatic substituted naphthalimides as potential antitumor agents: synthesis via Suzuki reaction, antiproliferative activity, and DNA-binding behavior', *Bioorg. Med. Chem.*, 2011, **4**, (2), pp. 961–967

[7] Shaista, P., Muhammad, S.S., Sumera, Z., *et al.*: 'Modification of Bischler–Möhlau indole derivatives through palladium catalyzed Suzuki reaction as effective cholinesterase inhibitors, their kinetic and molecular docking studies', *Bioorg. Chem.*, 2018, **76**, pp. 166–176

[8] Fedor, V.D., Georgii, V.C., Aziz, M.M.: 'The Suzuki modification of functional polydimethylsiloxanes', *Mendeleev Commun.*, 2017, **27**, (6), pp. 570–571

[9] Du, F., Zhang, L., Ma, J., *et al.*: 'Hemicelluloses supported palladium/xylan nanocomposites containing N and O ligands: highly-performance heterogeneous catalysts for Suzuki reaction', *Carbohydr. Polym.*, 2019, **217**, pp. 224–231

[10] Wang, Y., Lu, C., Wang, F., *et al.*: 'Main-chain diphosphine–Pd polymers: efficient self-supported heterogeneous catalysts for Suzuki–Miyaura reaction', *Mol. Catal.*, 2017, **437**, pp. 89–94

[11] Heidari, F., Hekmati, Ma., Veisi, H.: 'Magnetically separable and recyclable Fe_3O_4@SiO_2/isoniazide/Pd nanocatalyst for highly efficient synthesis of biaryls by Suzuki coupling reactions', *J. Colloid Interface Sci.*, 2017, **501**, pp. 175–184

[12] Li, J., Bai, X., Lv, H.: 'In-situ ultrasonic synthesis of palladium nanorods into mesoporous channel of SBA-15 and its enhanced catalytic activity for Suzuki coupling reaction', *Micropor. Mesopor. Mater.*, 2019, **275**, pp. 69–75

[13] Liu, Y., Bai, X., Li, S.: 'In-situ preparation of Pd nanoparticles in the pore channel of CMK-3 for Suzuki coupling reaction', *Micropor. Mesopor. Mater.*, 2018, **260**, pp. 40–44

[14] Nasrin, G., Farid, J., Roya, Z.: 'CuO and Ag/CuO nanoparticles: biosynthesis and antibacterial properties', *Mater. Lett.*, 2017, **196**, pp. 78–82

[15] Zhuang, Z., Wang, F., Ravendra, N., *et al.*: 'Biosynthesis of Pd–Au alloys on carbon fiber paper: towards an eco-friendly solution for catalysts fabrication', *J. Power Sources*, 2015, **291**, pp. 132–137

[16] Salehi, M.H., Yousefi, M., Hekmati, M., *et al.*: 'In situ biosynthesis of palladium nanoparticles on Artemisia abrotanum extract-modified graphene oxide and its catalytic activity for Suzuki coupling reactions', *Polyhedron*, 2019, **165**, pp. 132–137

[17] Yang, W., Ma, Y., Tang, J., *et al.*: ''Green synthesis' of monodisperse Pt nanoparticles and their catalytic properties', *Colloids Surf. A*, 2007, **302**, (1–3), pp. 628–633

[18] Lu, F., Sun, D., Huang, J., *et al.*: 'Plant-mediated synthesis of Ag–Pd alloy nanoparticles and their application as catalyst toward selective hydrogenation', *ACS Sustainable Chem. Eng.*, 2014, **02**, pp. 1212–1218

[19] Cai, Z., Liu, C., Wu, G., *et al.*: 'Green synthesis of Pt-on-Pd bimetallic nanodendrites on graphene via in situ reduction, and their enhanced electrocatalytic activity for methanol oxidation', *Electrochim. Acta*, 2014, **127**, pp. 377–383

[20] Weng, X., Guo, M., Luo, F.: 'One-step green synthesis of bimetallic Fe/Ni nanoparticles by eucalyptus leaf extract: biomolecules identification, characterization and catalytic activity', *Chem. Eng. J.*, 2017, **308**, pp. 904–911

© The Institution of Engineering and Technology 2019

[21] Naik, G.K., Mishra, P.M., Parida, K.: 'Green synthesis of Au/TiO_2 for effective dye degradation in aqueous system', *Chem. Eng. J.*, 2013, **229**, pp. 492–497
[22] Yadav, S., Khurana, J.M.: 'Cinnamomum tamala leaf extract-mediated green synthesis of Ag nanoparticles and their use in pyranopyrazles synthesis', *Chin. J. Catal.*, 2015, **36**, (7), pp. 1042–1046
[23] Park, S., Park, D., Kang, J.Y.: 'Influence of the preparation method on the catalytic activity of MgAl hydrotalcites as solid base catalysts', *Green Energy Environ.*, 2019, **4**, (3), pp. 287–292
[24] Raoudha, Y., Pedro, E.S.J., Luis, A.P.M.: 'Synthesis, characterization and combined kinetic analysis of thermal decomposition of hydrotalcite ($Mg_6Al_2(OH)_{16}CO_3{\cdot}4H_2O$)', *Thermochim. Acta*, 2018, **667**, pp. 177–184
[25] Burrueco, M.I., Mora, M., Ruiz, J.R.: 'Hydrotalcite-supported palladium nanoparticles as catalysts for the Suzuki reaction of aryl halides in water', *Appl. Catal., A*, 2014, **485**, pp. 196–201
[26] Northup, R.R., Yu, Z., Dahlgren, R.A*., et al.*: 'Polyphenol control of nitrogen release from pine litter', *Nature*, 1995, **377**, (6546), pp. 227–229
[27] Liu, G., Bai, X.: 'Biosynthesis of palladium nanoparticles using poplar leaf extract and its application in Suzuki coupling reaction', *IET Nanobiotechnol.*, 2017, **11**, (3), pp. 310–316
[28] Yang, X., Li, Q., Wang, H*., et al.*: 'Green synthesis of palladium nanoparticles using broth of Cinnamomum camphora leaf', *J. Nanoparticle Res.*, 2010, **12**, pp. 1589–1598
[29] Feng, J.T., Ma, X.Y., He, Y.F*., et al.*: 'Synthesis of hydrotalcite-supported shape-controlled Pd nanoparticles by a precipitation–reduction method', *Appl. Catal. A*, 2012, **413–414**, pp. 10–20
[30] Naresh, D., Kumar, V.P., Harisekhar, M*., et al.*: 'Characterization and functionalities of Pd/hydrotalcite catalysts', *Appl. Surf. Sci.*, 2014, **314**, pp. 199–207
[31] Andrés, F.S., Li, W.S.J., Bathfield, M*., et al.*: 'Hierarchically porous Pd/SiO_2 catalyst by combination of miniemulsion polymerisation and sol-gel method for the direct synthesis of H_2O_2', *Catal. Today.*, 2018, **306**, pp. 16–22
[32] Mahmoud, N., Sajadi, S.M., Akbar, R.V*., et al.*: 'Green synthesis of Pd/Fe_3O_4 nanoparticles using *Euphorbia condylocarpa* M. Bieb root extract and their catalytic applications as magnetically recoverable and stable recyclable catalysts for the phosphine-free Sonogashira and Suzuki coupling reactions', *J. Mol. Catal. A, Chem*, 2015, **396**, pp. 31–39
[33] Mahmoud, N., Sajadi, S.M., Akbar, R.V*., et al.*: 'Green synthesis of Pd/CuO nanoparticles by *Theobroma cacao* L. seeds extract and their catalytic performance for the reduction of 4-nitrophenol and phosphine-free Heck coupling reaction under aerobic conditions', *J. Colloid Interface Sci.*, 2015, **448**, pp. 106–113
[34] Nasrollahzadeh, M., Sajadi, S.M.: 'Pd nanoparticles synthesized in situ with the use of Euphorbia granulate leaf extract: catalytic properties of the resulting particles', *J. Colloid Interface Sci.*, 2016, **462**, pp. 243–251
[35] Trzeciak, A.M., Augustyniak, A.W.: 'The role of palladium nanoparticles in catalytic C–C cross-coupling reactions', *Coord. Chem. Rev.*, 2019, **384**, pp. 1–20
[36] Das, P., Linert, W.: 'Schiff base-derived homogeneous and heterogeneous palladium catalysts for the Suzuki–Miyaura reaction', *Coord. Chem. Rev.*, 2016, **311**, pp. 1–23

6 Appendix

6.1 Determining the content of phenols in the WWL

The Graham method is used to determine the amount of phenolic content in the WWL. Specific steps are as follows: (i) a 2 mol/l solution was formed, which contains 0.02 g gallic acid and 10 ml distilled water in a volumetric flask. (ii) The gallic acid solution was diluted to different gradients with the UV–Vis to detect the absorbance, and the linear equation ($Y = 0.00545 + 0.0446X$) was derived by the correlation of concentration and absorbance. (iii) The yield of phenols in the extract was notarised by the linear equation, whose absorbance was obtained by the ultraviolet spectrograph (Fig. 11 and Table 4).

6.2 Particle size distribution of catalysts

See Fig. 12.

© The Institution of Engineering and Technology 2019

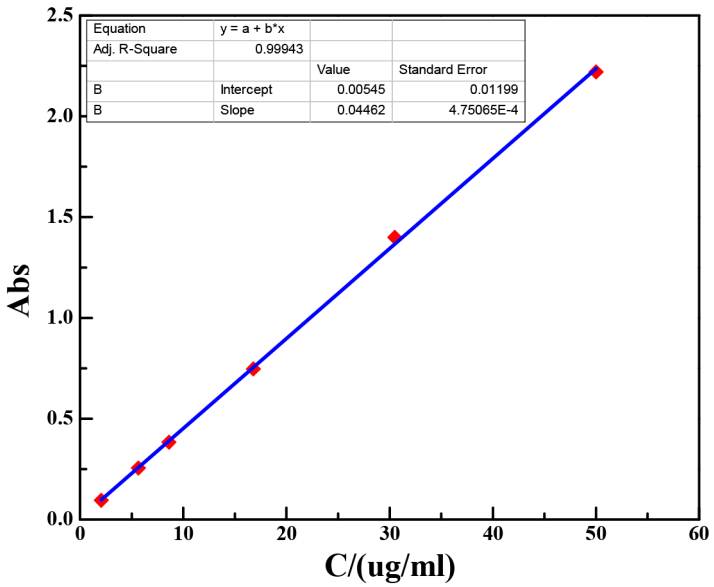

Fig. 11 *Standard curve and equation of gallic acid*

Table 4 Experiment conditions and change of biomass content

No.	*T*, °C	Time, min	Content[a], %
1	10	60	2.25
2	20	60	5.86
3	30	60	8.81
4	40	60	12.23
5	50	60	19.06
6	60	60	22.72
7	70	60	23.11
8	80	60	23.35
9	60	10	6.89
10	60	20	13.07
11	60	30	18.59
12	60	90	23.90
13	60	120	24.08

[a]Absorbance of biomass × 100% /absorbance of gallic acid (with the same mass concentration).

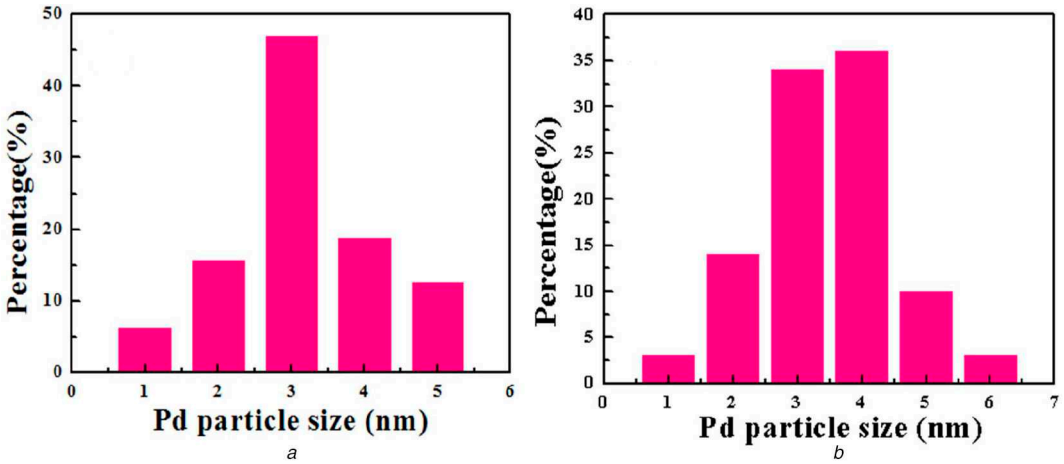

Fig. 12 *Particle size distribution of*
(a) Pd/LDHs-B, ***(b)*** Pd/LDHs-P

© The Institution of Engineering and Technology 2019